

# Predictive Control of Aerial Swarms in Cluttered Environments

Enrica Soria, Fabrizio Schiano, and Dario Floreano<sup>1\*</sup>

**Abstract.** Classical models of aerial swarms often describe global coordinated motion as the combination of local interactions that happen at the individual level. Mathematically, these interactions are represented with Potential Fields. Despite their explanatory success, these models fail to guarantee rapid and safe collective motion when applied to aerial robotic swarms flying in cluttered environments of the real world, such as forests and urban areas. Moreover, these models necessitate a tight coupling with the deployment scenarios to induce consistent swarm behaviors. Here, we propose a predictive model that incorporates the local principles of potential field models in an objective function and optimizes those principles under the knowledge of the agents' dynamics and environment. We show that our approach improves the speed, order, and safety of the swarm, it is independent of the environment layout and scalable in the swarm speed and inter-agent distance. Our model is validated with a swarm of five quadrotors that can successfully navigate in a real-world indoor environment populated with obstacles.

## 1 Introduction

From the fluid wavelike movements of starling flocks to the swift turning maneuvers of bee swarms, nature displays many examples of coordinated flight [1]–[7]. Recent progress in aerial robotics technologies led to the availability of smart drones at the price of smartphones [8], but the deployment of drone swarms that autonomously coordinate their local trajectories remains a challenge. Drone swarms can offer larger area coverage than a single drone for monitoring and exploration missions [9], [10], and they can collect multi-dimensional sensory data by flying a diverse set of sensors [11]. Autonomous aerial swarms can also enable functionalities that are beyond the capabilities of a single drone, such as cooperative transportation of large objects and aerial construction [12], [13]. Hundreds of drones have been deployed in aerial light shows by companies such as Intel [14], EHang [15], and Verity Studios [16], but in those circumstances, every drone is individually controlled by a central computer to follow a precomputed trajectory. Instead, the coordinated, synchronized motion of biological swarms is a self-organized behavior that emerges from local information [4]–[6], [17]–[19], and can thus cope with unforeseen situations, such as flying through forests or in urban canyons.

Early work suggested that the collective motion of a biological swarm can be described by the combination of three behavioral rules that apply to each agent simultaneously [20]. These rules consist of (a) *cohesion*, which brings each agent closer to its neighbors, (b) *repulsion*, which drives each agent away from its neighbors to avoid collisions, and (c) *alignment*, which steers each agent towards the average heading of its neighbors. In goal-directed flight, alignment is replaced by *migration*, which steers each agent in a preferred migration direction [21], [22]. For

---

<sup>1</sup> The authors are from the Laboratory of Intelligent Systems (LIS), École Polytechnique Fédérale de Lausanne (EPFL), Lausanne, Switzerland.

\* E-mail: [enrica.soria@epfl.ch](mailto:enrica.soria@epfl.ch), [fabrizio.schiano@epfl.ch](mailto:fabrizio.schiano@epfl.ch), [dario.floreano@epfl.ch](mailto:dario.floreano@epfl.ch)

42 navigating environments with obstacles, the addition of a fourth rule, *collision avoidance*, is  
43 necessary to steer the agents around the obstacles [20], [23], [24]. Although these rules are  
44 defined locally, i.e., every agent regulates its flight with respect to a limited set of neighboring  
45 agents, they have proven to produce a globally coordinated motion. Mathematically, these rules  
46 can be modeled by virtual forces exerted by the agents on their neighbors and are associated  
47 with Potential Fields (PFs), i.e., vector fields describing how forces act at various positions  
48 in space. PFs encode the desired behaviors of the swarm. They regulate the inter-agent distance  
49 among neighboring individuals similarly to a spring-mass system, adjust the velocity of the  
50 agents, steer them towards a common direction, and regulate their distance to obstacles [23].  
51

52 The advantage of PF swarm models is that they are purely reactive, meaning that their decisions  
53 are solely based on the current sensory information and thus have low computational  
54 complexity [20], [23]. For this reason, PF models are convenient for the implementation on real  
55 robotic systems, either in free environments [21], [25], or in environments with convex  
56 obstacles [24]. In the latter case, collision avoidance is obtained by defining virtual repulsive  
57 agents (called *shill agents*) located along the obstacles' boundaries. However, these *shill agents*  
58 present the inconvenience of slowing down the swarm as it approaches the obstacles [20], [26].  
59 This effect becomes prominent in environments with high obstacle densities, where PF swarms  
60 can significantly slow down. The slowdown can be attenuated by weakening the repulsion  
61 potentials, albeit at the expense of the swarm safety, because some agents may collide.  
62 Moreover, to account for the idiosyncrasies of the real world, these models often include a  
63 significant number of parameters that have complex interdependencies [2], [24]. As a  
64 consequence, they often require the adoption of optimization techniques such as evolutionary  
65 algorithms, to identify a viable instantiation of the parameters, and each instantiation is specific  
66 to the swarm's preferred speed and inter-agent distance and to the environmental layout [21],  
67 [24], [27].  
68

69 Here we propose a method to remove those difficulties that consist of endowing swarming  
70 agents with prediction-based control. Specifically, we show that aerial swarms with predictive  
71 control display faster flight while guaranteeing safe navigation in cluttered environments, they  
72 can adapt to diverse obstacle densities, and they are scalable to changes in the inter-agent  
73 distance and swarm's speed. It has been recently advocated that some form of predictive  
74 control, in the form of an internal model of the actions of their conspecifics, may also be  
75 leveraged by biological swarms where the apparent synchronization of coordinated maneuvers,  
76 such as a flock of starlings or a school of fish, cannot be explained by a purely reactive system  
77 [19]. Inspired by this hypothesis, the method proposed in this paper endows flying agents with a  
78 model of swarm behavior based on Nonlinear Model Predictive Control (NMPC).  
79

80 Model Predictive Control (MPC) is a method that computes the control action of a system as the  
81 solution of a constrained optimization problem [28], [29]. MPC leverages a mathematical  
82 representation of the system to predict and optimize its future behavior in an iterative process.  
83 Differently from PF control, MPC can explicitly handle constraints, such as physical limitations  
84 (e.g., flight speed and acceleration ranges of a drone) [30]–[32], and environmental restrictions  
85 (e.g., no-flight zones) [32]–[34]. However, the recursive online solution of constrained

86 optimization problems is associated with higher computational costs, and therefore the  
87 adoption of predictive controllers in robotics has spread only recently [35].

88  
89 MPC has shown promising results in simulation on multi-vehicle systems. Examples include the  
90 stabilization of multiple agents in obstacle-free environments [36], [37], in the presence of  
91 obstacles [33], and the generation of collision-free trajectories for groups of robots with known  
92 target locations [38]–[40]. NMPC is a variant of MPC that can handle the nonlinearities of a  
93 system or its constraints [29]. This advantage comes at the cost of being more computationally  
94 demanding. In the simulation, NMPC has been used to control leader-follower formations of  
95 drones without obstacles [41], and to control 2D quadrotor formations in the presence of  
96 convex obstacles [34].

97  
98 Less work has been done on the use of MPC with multiple real drones, notably due to the  
99 difficulty of real-time implementation. Linear MPC has been used for trajectory planning in the  
100 presence of virtual obstacles in a leader-follower configuration, where a drone (the follower)  
101 has to keep a constant distance from a virtual agent (the leader), [42]. However, in leader-  
102 follower approaches, the leader has the extra knowledge of the group trajectory, which is either  
103 preprogrammed or provided by an external source. This aspect introduces an asymmetry in the  
104 agents' roles and adds a single point of failure in the swarm [43]. MPC has been used for the  
105 online generation of collision-free trajectories for a group of drones in environments with  
106 obstacles, where every drone is individually assigned an initial position and a target destination  
107 [32]. Instead, the model presented here is meant to coordinate the navigation of the swarm as a  
108 unique entity and guarantee internal order, in lieu of generating the trajectories separately.  
109 Concurrently, we avoid imposing a rigid formation or a fixed topology to the swarm, which may  
110 impact the freedom and fluidity of the agents' movements. Finally, NMPC has been shown to be  
111 capable of dealing with non-convex collision avoidance constraints in real multi-drone systems  
112 when the agents are assigned intersecting paths, although they were flying in empty  
113 environments [44].

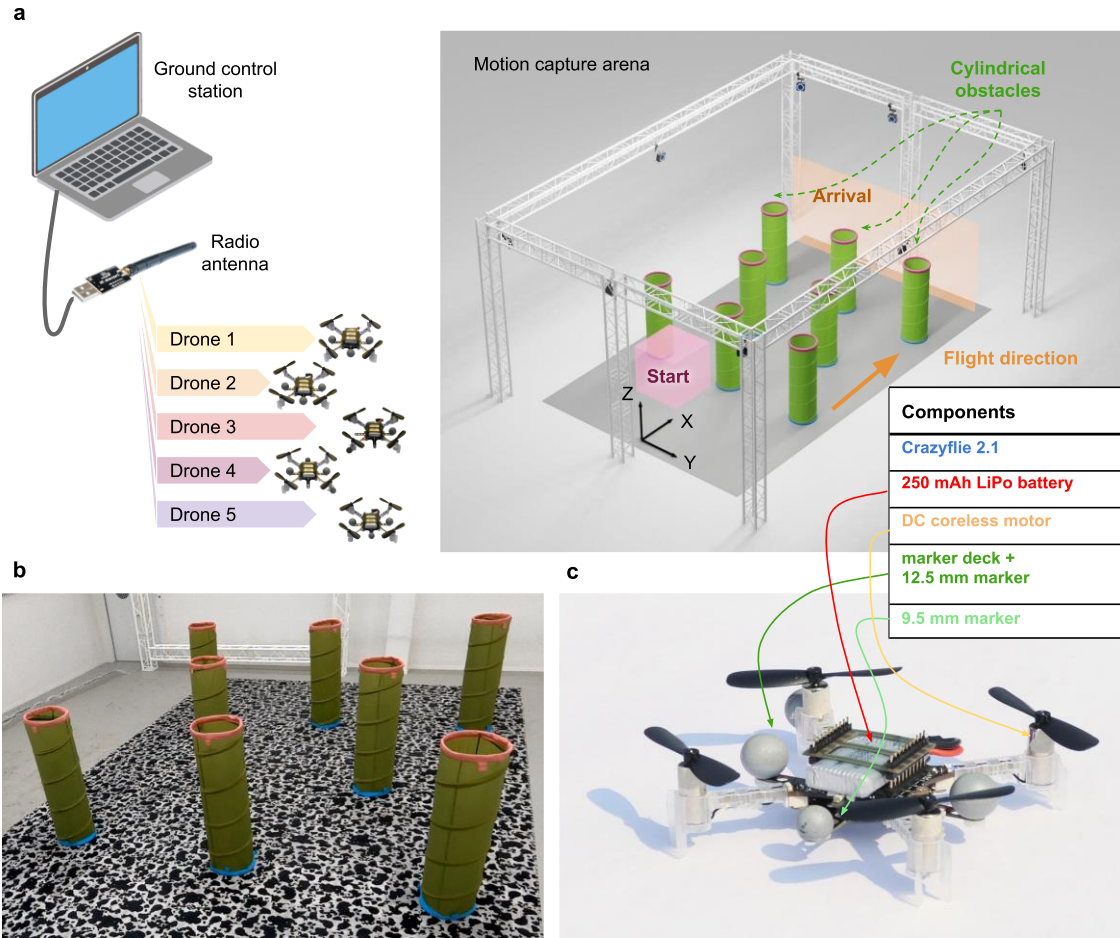
114  
115 In the proposed NMPC model, the objective function to be optimized is made of three  
116 components inspired from PF swarm models: (a) *separation*, which drives the inter-agent  
117 distances to a preferred value, (b) *propulsion*, which propels the agents with a preferred speed  
118 value, and (c) *direction*, which steers the swarm along a preferred direction. The separation  
119 component incorporates the effects of cohesion and repulsion in a single rule, in such a way  
120 that the inter-agent distance between neighboring individuals appears as an explicit parameter.  
121 The propulsion and direction components taken together in the NMPC swarm model replicate  
122 the effect of the migration term in the PF swarm models. However, keeping two terms with two  
123 independent parameters allows separate adjustments of their relative strengths. A fourth rule,  
124 (d) *control effort* is added to minimize the agents' accelerations, thereby smoothing flight  
125 trajectories and increasing energy efficiency. Each drone regulates its flight based on the  
126 knowledge of its neighbors and its own state and predicts its own trajectory and those of its  
127 neighbors thanks to a linearized dynamical model. The drones' neighbors are selected within a  
128 topological range, i.e. for every drone only a constant number of nearest neighbors is  
129 considered [3], [7]. The proposed NMPC model integrates a set of constraints to ensure safety

130 distances among drones and with obstacles. We implement a centralized version of our NMPC  
131 model and we compare simulation results to a PF model. We show that predictive controllers  
132 can safely fly the swarm in cluttered environments while significantly increasing the flight speed  
133 and synchronization of the swarm. Also, we show that the performance of the proposed NMPC  
134 model is independent of the obstacle density and environmental layout, differently from PF  
135 models. Additionally, we test the scalability of the proposed model to variations of desired  
136 inter-agent distance and swarm speed. We perform systematic experiments in simulation and  
137 validate the results with a swarm of five palm-sized quadrotors.  
138

## 139 2 Results

140  
141 For the performance assessment of the swarm models, we set up a forest-like environment that  
142 consists of a rectangular flight region populated with cylindrical obstacles (Fig. 1a). At the  
143 experiment onset, we place five drones at random positions within a predefined start area on  
144 one side of the region (Fig. 1a, red zone) and let the swarm fly through the region along the  
145 migration direction (Fig. 1a, orange arrow). The mission is completed when all drones cross the  
146 arrival plane (Fig. 1a, orange plane) on the opposite side of the region.  
147

148 We assess the quality of the aerial swarm’s flight considering eight different metrics. The  
149 mission completion time  $T$  measures the time that the swarm requires to cross the region. The  
150 inter-agent distance error  $E_d$  measures the agents’ deviation from the preferred distance  
151  $d_{\text{ref}}$ , and the inter-agent distance range  $R_d$  measures the range in which the inter-agent  
152 distances vary (defined by the minimum and maximum inter-agent distance over time). The  
153 speed error  $E_v$  measures the deviation of the agents’ speeds from the preferred migration  
154 speed  $v_{\text{ref}}$ , and the speed range  $R_v$  measures the range in which the agents’ speeds vary.  $E_d$ ,  
155  $R_d$ ,  $E_v$  and  $R_v$  take values greater than or equal to 0 (ideal case). We determine the swarm’s  
156 level of synchronization by calculating the directional correlation of the agents’ movements,  
157 expressed by the so-called order  $\Phi_{\text{order}}$ .  $\Phi_{\text{order}}$  takes values between  $-1$  (complete  
158 disorder) and  $1$  (perfect order). Finally, the agent-agent safety  $\Phi_{\text{agent-safety}}$  assesses the  
159 ability of the swarm’s agents to avoid collisions among themselves, and the agent-obstacle  
160 safety  $\Phi_{\text{obs-safety}}$  assesses the ability of the agents to avoid collisions with the obstacles.  
161  $\Phi_{\text{agent-safety}}$  and  $\Phi_{\text{obs-safety}}$  take values between 0 (complete unsafety) and 1 (perfect  
162 safety, i.e., zero collisions) (see Supplementary Table 1 for mathematical formulation). To  
163 evaluate the overall performance of the swarm during a mission, we compute the average and  
164 standard deviation of these metrics. For the instantaneous evaluation of the swarm over time,  
165 we additionally plot the inter-agent distance and speed, and the distance to obstacles, from  
166 which we can appreciate their respective errors and ranges, and the occurrence of collisions.  
167



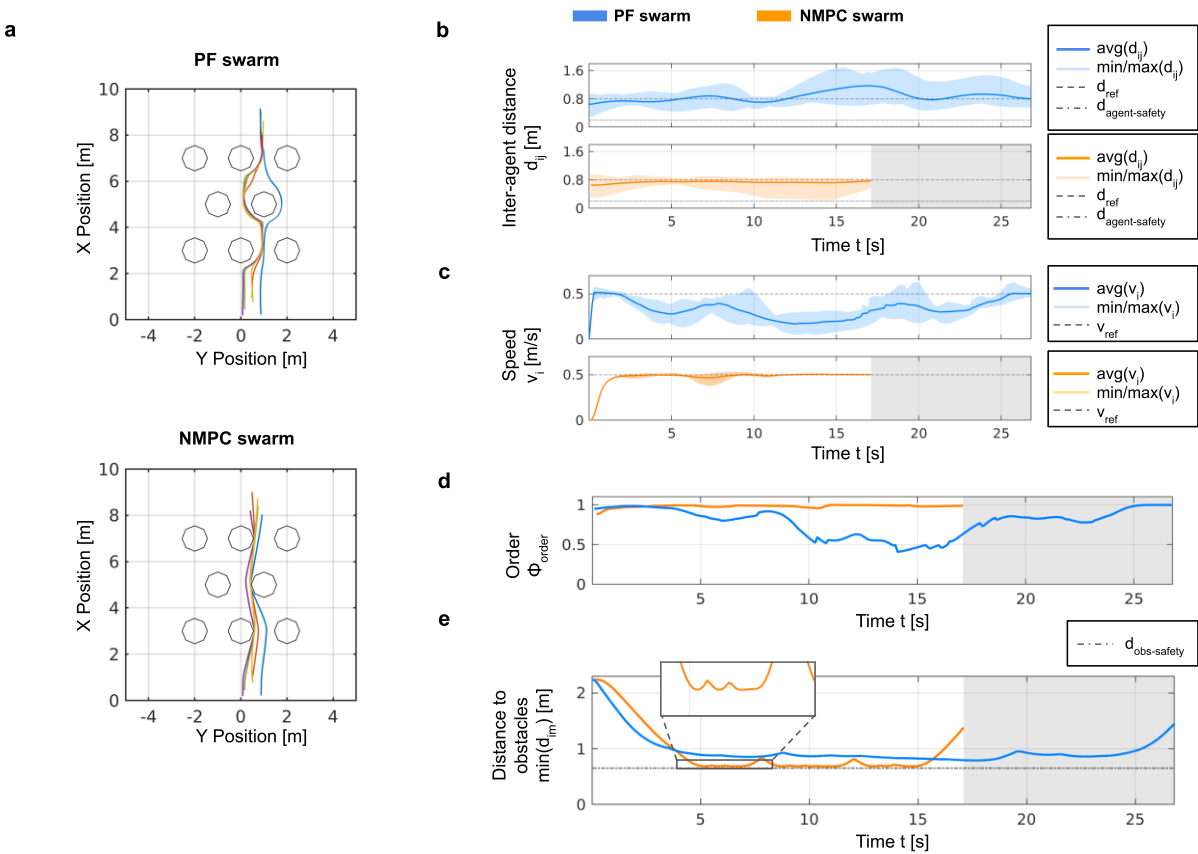
168 Fig. 1: **Experimental setup of drone swarm flight in cluttered environments.** (a) Illustration of  
 169 the experimental setup and the environment configuration. A ground control station, equipped  
 170 with a radio transmitter, computes and sends run-time control commands to the drones. The  
 171 swarm flies in the 3D space of an indoor flying arena. The drones take off from initial random  
 172 positions within a predefined start area (red zone). Drones swarm along the preferred migration  
 173 direction (orange arrow). The mission is completed when all drones cross the arrival plane (Fig.  
 174 1a) on the opposite side of the region. (b) Indoor test environment populated with cylindrical  
 175 obstacles. (c) Components of the drones used for the hardware experiments.

176  
 177 We extensively tested the proposed NMPC swarm model in simulation and compared it to a  
 178 reactive PF model that has been recently described and validated on 30 real drones [24]. In  
 179 addition to the repulsion and obstacle avoidance rules, the PF model includes a *friction* rule to  
 180 reduce velocity oscillations. In order to ensure cohesive goal-directed flight in open  
 181 environments, we added the rules of *cohesion* and *migration* to the PF model. As in previous  
 182 work [21], [24], [27], we used evolutionary optimization to search the large parameter space of  
 183 the PF swarm model, and favored swarms with highly ordered flight ( $\Phi_{\text{order}} = 1$ ) and a low  
 184 number of agent-agent and agent-obstacle collisions ( $\Phi_{\text{agent-safety}} = 1$ ,  $\Phi_{\text{obs-safety}} = 1$ ) (see  
 185 Supplementary Table 3). The purpose of the experimental comparison between NMPC

186 swarming and PF swarming is to emphasize behavioral differences and performance advantages  
 187 of the proposed NMPC swarm model. However, the choice of a swarm model for the  
 188 deployment on physical drones should also consider computational resources, which are  
 189 significantly larger for NMPC swarming.

191 Below we present three sets of simulation experiments: (i) we compare the performance  
 192 metrics of the two models in the same environmental conditions, (ii) we investigate the  
 193 adaptability of the PF and NMPC swarm models to environments with different obstacle  
 194 density, and (iii) we study the scalability of the NMPC swarm model at different preferred  
 195 speeds and inter-drone distances. Finally, we experimentally validate the NMPC swarm model  
 196 with five palm-sized drones (Fig. 1c) flying through a room with cylindrical obstacles (Fig. 1b).  
 197

## 198 2.1 Comparison of PF and NMPC aerial swarms



200  
 201  
 202 **Fig. 2: Comparison of the PF and NMPC aerial swarms in simulation experiments. (a)** Top views  
 203 of the 3D trajectories of five drones flying in a cluttered environment with the PF (top) and the  
 204 NMPC models (bottom) (see Supplementary Video 1). The circular objects on the map  
 205 correspond to cylindrical obstacles. **(b)** Inter-agent distance average (solid line) and range  
 206 (shaded region). The curve on top (blue) refers to the PF swarm, while the one at the bottom  
 207 (orange) refers to the NMPC swarm. **(c)** Swarm speed average (solid line) and range (shaded

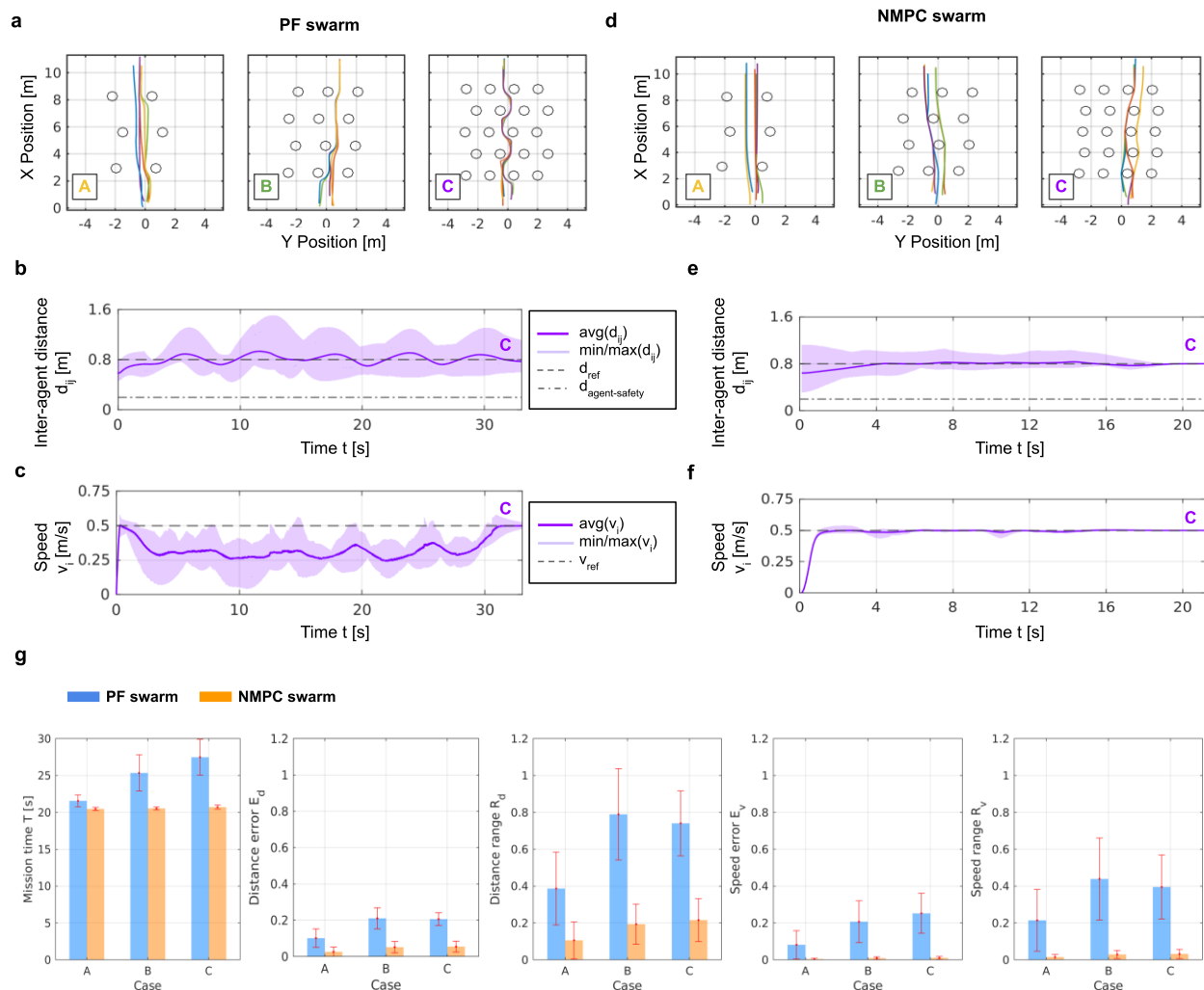
208 region). **(d)** Order metric. **(e)** Distance to obstacles,  $\min(d_{im})$ , expressed as the minimum  
209 distance between the swarm's agents and the set of obstacles.

210  
211 Both PF and NMPC swarms navigated around the obstacles without collisions (Fig. 2e), but the  
212 NMPC swarm completed the mission 57% faster than the PF swarm. The reduced mission time is  
213 due to the ability of the NMPC swarm to track the preferred speed  $v_{ref}$  more consistently ( $E_v =$   
214  $0.02 \pm 0.02$ ,  $R_v = 0.08 \pm 0.07$ ) than PF swarm ( $E_v = 0.39 \pm 0.15$ ,  $R_v = 0.47 \pm 0.15$ ) (Fig. 2c). The  
215 NMPC swarm also generated a smaller inter-agent distance error ( $E_d = 0.11 \pm 0.02$ ) and range  
216 ( $R_d = 0.55 \pm 0.18$ ) compared to the PF swarm ( $E_d = 0.26 \pm 0.15$ ,  $R_d = 0.90 \pm 0.26$ ) (Fig. 2b).  
217 The NMPC model generated almost perfectly ordered flight manoeuvres throughout the entire  
218 flight ( $\Phi_{order} = 0.98 \pm 0.02$ ) while the PF model displayed lower and more variable order  
219 ( $\Phi_{order} = 0.78 \pm 0.17$ ) (Fig. 2d). Neither the NMPC nor the PF swarm presented agent-agent  
220 or agent-obstacle collisions ( $\Phi_{agent-safety} = 1 \pm 0$ ,  $\Phi_{obs-safety} = 1 \pm 0$ ) (Fig. 2e). While  
221 optimizing the swarm's objectives, the NMPC model reduced the minimum distance to  
222 obstacles to  $0.03 m$ . In comparison, the PF swarm achieved a minimum distance to obstacles of  
223  $0.14 m$ . This difference is due to the fact that in the PF model the obstacles apply a repulsion  
224 force on the agents in their proximity, while in the NMPC model there is no penalty for  
225 approaching the obstacles. As a consequence, when implementing the NMPC model on a real-  
226 world swarm, the user should carefully choose a safety margin.

227

## 228 **2.2 Environments with different obstacle densities**

229



230  
 231  
 232 **Fig. 3: Comparison of the PF and NMPC swarm deployment in environments with different**  
 233 **obstacle densities. (a, d) Top views of the 3D simulated trajectories of the PF and the NMPC**  
 234 **swarms in environments with three different obstacle densities. The density increases from left**  
 235 **to right (Case A: 0.06, B: 0.12, and C: 0.20) (see Supplementary Video 1). (b, c) Inter-agent**  
 236 **distance and speed of the PF swarm in Case C. (e, f) Inter-agent distance and speed of the NMPC**  
 237 **swarm in Case C. (g) Aggregated results (average and standard deviation) of 10 stochastic**  
 238 **simulations of the PF (blue) and NMPC (orange) swarm models in Cases A, B, and C. The**  
 239 **represented metrics are the mission time  $T$ , the distance error  $E_d$ , the distance range  $R_d$ , the**  
 240 **speed error  $E_v$ , and the speed range  $R_v$  (see Supplementary Table 1).**  
 241

Parameter	Unit	Description	Value
$d_{ref}$	$m$	Preferred (or reference) value for the inter-agent distance	0.8
$v_{ref}$	$m/s$	Preferred (or reference) value for the swarm speed	0.5
$\mathbf{u}_{ref}$	-	Preferred migration direction	(1 0 0)

$L_{\text{map}}$	$m$	Length of an edge of the square flight region (or map)	10
$r_{\text{obs}}$	$m$	Obstacles radius	0.35
$\rho_{\text{obs}}$	$-/m^2$	Obstacle density	Case A: 0.06 Case B: 0.12 Case C: 0.20

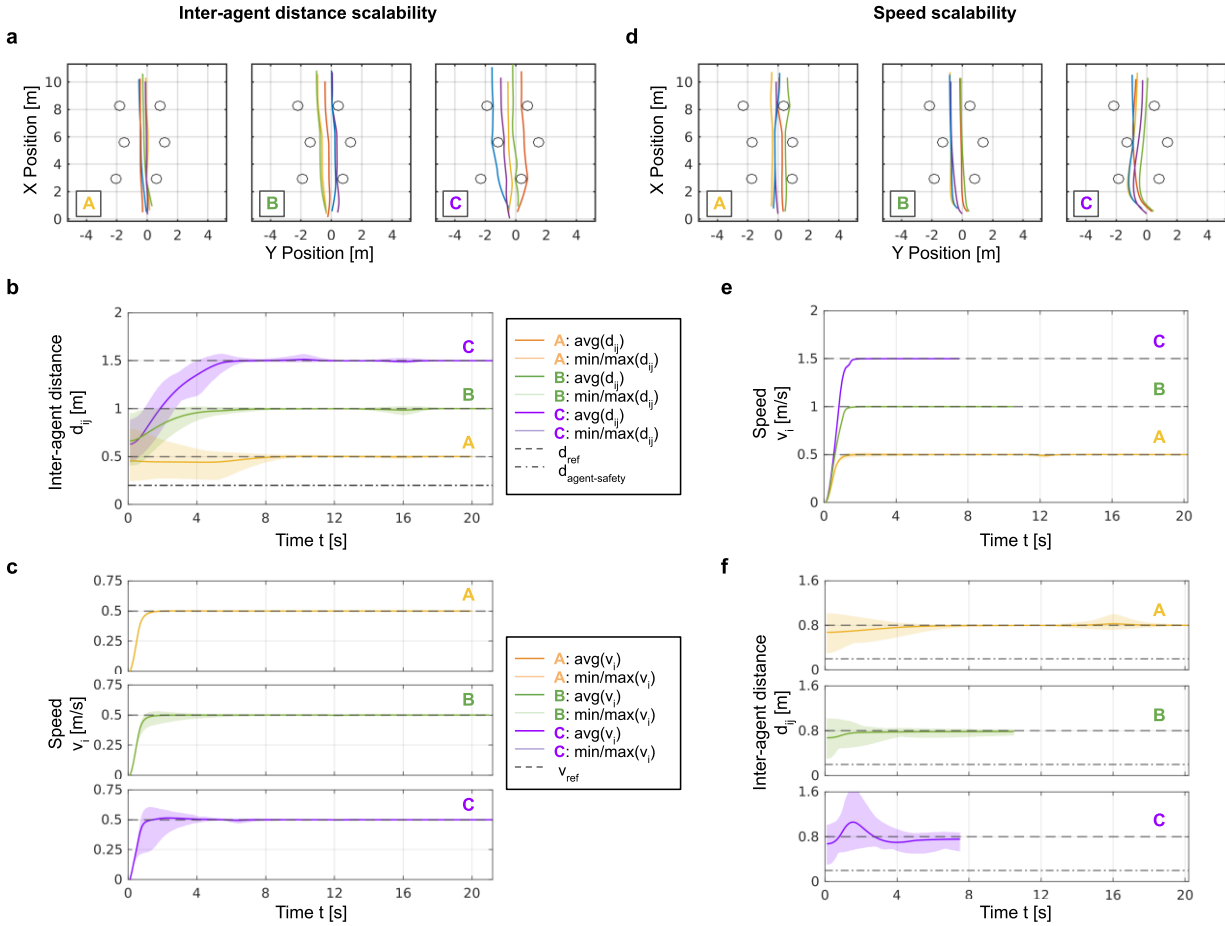
242  
243 **Table 1: Swarm and environment configurations of the simulation experiments with different**  
244 **obstacle densities.** The same configurations are used for both the PF and the NMPC swarm  
245 models.  
246

247 We tested the PF and the NMPC swarm models for three different obstacle densities (Case A:  
248 0.06, B: 0.12, and C: 0.20) to quantify the impact on the swarms' performance. The obstacles  
249 occupy random positions on the map, but they have a homogenous distribution (Fig. 3a and 3d).  
250 The initial positions of the drones are random. In Fig. 3, we show the evolution of the inter-  
251 agent distance and speed for the scenario with the highest obstacle density (Case C) and for  
252 both models. The results show that the inter-agent distance error is smaller with NMPC swarms  
253 ( $E_d = 0.11 \pm 0.02$ ) than with PF swarms ( $E_d = 0.27 \pm 0.12$ ), and the inter-agent distance  
254 range is shorter for NMPC swarms ( $R_d = 0.56 \pm 0.18$ ) than with PF swarms ( $R_d = 0.90 \pm$   
255  $0.26$ ) (Fig. 3b and 3e). The NMPC swarms tracked the preferred speed  $v_{\text{ref}}$  more precisely  
256 ( $E_v = 0.03 \pm 0.02$ ) than the PF swarms ( $E_v = 0.39 \pm 0.15$ ), and the speed range was shorter  
257 ( $R_v = 0.08 \pm 0.07$  and  $0.47 \pm 0.15$ , respectively) (Fig. 3c and 3f). The faster speed of NMPC  
258 swarms resulted in faster mission completion time than the PF swarms ( $T = 21.5$  s and  $34.1$  s,  
259 respectively).  
260

261 To assess the reproducibility of the results, we performed ten stochastic simulations for each of  
262 the three obstacle densities and for the two swarm models, and we report here aggregated  
263 performance results (Fig. 3g). While the speed error in the NMPC swarm is small and constant  
264 for all obstacle densities (Case A:  $E_v = 0.01 \pm 0.01$ , B:  $0.01 \pm 0.01$ , C:  $0.01 \pm 0.01$ ), it is  
265 larger and increases with larger obstacles densities in the PF swarm (Case A:  $E_v = 0.08 \pm 0.07$ ,  
266 B:  $0.21 \pm 0.11$ , C:  $0.25 \pm 0.11$ ). As a consequence, the mission completion time of the PF  
267 swarm is increased when increasing the obstacle density (Case A:  $T = 21.56 \pm 0.81$  s, B:  
268  $25.35 \pm 2.46$  s, C:  $27.48 \pm 2.43$  s), while for the NMPC swarm it is shorter and it stays almost  
269 constant across the different densities (Case A:  $T = 20.47 \pm 0.22$  s, B:  $20.54 \pm 0.21$  s, C:  
270  $20.72 \pm 0.28$  s). Also, the PF swarm's order deteriorates when increasing the obstacle density  
271 (Case A:  $\Phi_{\text{order}} = 0.98 \pm 0.03$ , B:  $0.92 \pm 0.08$ , C:  $0.81 \pm 0.08$ ), while for the NMPC swarm it  
272 stays almost constant (Case A:  $\Phi_{\text{order}} = 0.99 \pm 0.01$ , B:  $0.98 \pm 0.02$ , C:  $0.98 \pm 0.02$ ). While  
273 the NMPC swarm produces collision-free movements in all cases, for the PF swarm we observe  
274 some agent-obstacle collisions at high obstacle densities (Case A:  $\Phi_{\text{obs-safety}} = 1 \pm 0$ , B:  
275  $(99.98 \pm 0.06) 10^{-2}$ , C:  $(99.99 \pm 0.02) 10^{-2}$ ). The aggregated performance results are  
276 summarized in Supplementary Table 5.  
277

### 278 **2.3 Scalability to different inter-agent distances and speeds**

279



281  
 282  
 283 **Fig. 4: Scalability of the NMPC swarm in inter-agent distance and speed.** On the left, simulation  
 284 results on the scalability of the NMPC swarm model in the inter-agent distance for three  
 285 preferred distance values (Case A:  $d_{ref} = 0.5 m$ , B:  $1.0 m$ , and C:  $1.5 m$ ). On the right,  
 286 simulation results on the scalability in the swarm speed for three preferred speed values (Case  
 287 A:  $v_{ref} = 0.5 m/s$ , B:  $1.0 m/s$ , and C:  $1.5 m/s$ ). **(a, d)** Top views of the 3D trajectories of the  
 288 swarm (see Supplementary Video 1). **(b, c)** Inter-agent distance and speed for the experiment  
 289 on the inter-agent distance scalability. **(e, f)** Inter-agent distance and speed for the experiment  
 290 on the speed scalability. The obstacle size and density are the same for the six cases.  
 291

292 We assess the scalability of the proposed NMPC model to different values of the preferred  
 293 inter-agent distance (Case A:  $d_{ref} = 0.5 m$ , B:  $1.0 m$ , and C:  $1.5 m$ , see Fig 4 a-c) and speed  
 294 (Case A:  $v_{ref} = 0.5 m/s$ , B:  $1.0 m/s$ , and C:  $1.5 m/s$ , see Fig 4 d-f) in the same environmental  
 295 conditions. We analyze the swarm's inter-agent distance and speed and quantify their  
 296 respective errors and ranges. The results show that at different inter-agent distance levels the  
 297 swarm inter-agent distance converged to the preferred value with comparable errors (Case A:  
 298  $E_d = 0.05 \pm 0.06$ , B:  $0.01 \pm 0.02$ , C:  $0.02 \pm 0.03$ , see Fig. 4b). The swarm's speed error is  
 299 almost zero in the three cases (see Fig. 4c), and it resulted in similar mission times (Case A:  $T =$

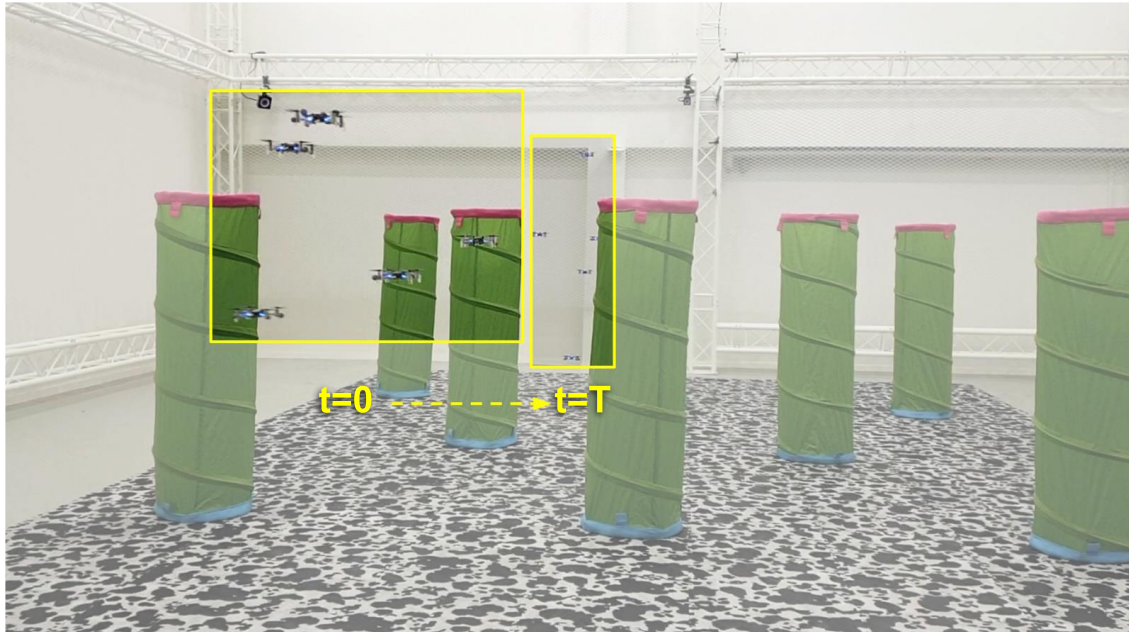
300 20 s, B: 21 s, and C: 21.2 s). We did not observe collisions. Regarding the experiments on the  
301 scalability in speed, the speed error  $E_v$  was close to zero in the three cases (Fig. 4e), while the  
302 mission times were decreasing with the increase of the speed (Case A:  $T = 20.2$  s, B: 10.5 s,  
303 and C: 7.5 s). However, the variability of the inter-agent distance in Case C is higher ( $R_d =$   
304  $0.46 \pm 0.05$ ) than in Cases A ( $R_d = 0.13 \pm 0.11$ ) and B ( $R_d = 0.19 \pm 0.03$ ) (Fig. 4f). Indeed,  
305 when the agents turn around the obstacle in the middle of the scene, they rearrange and  
306 increase their distance. Also in these experiments, we did not observe collisions. Comparative  
307 results on the PF swarm are in Supplementary Fig. 1. Aggregate results of stochastic simulations  
308 for each of the preferred inter-agent distance and speed values, and for both the PF and the  
309 NMPC models are in Supplementary Fig. 2, and in Supplementary Tables 6 and 7.

310

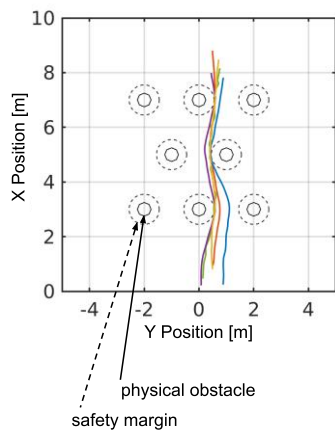
## 311 **2.4 Validation with real drones**

312

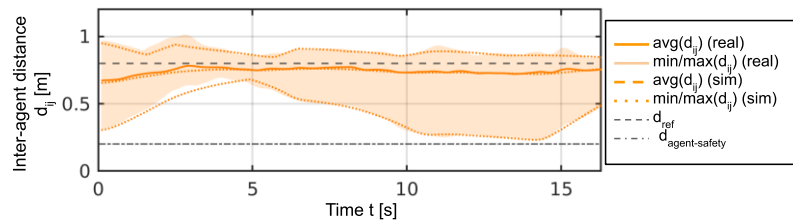
a



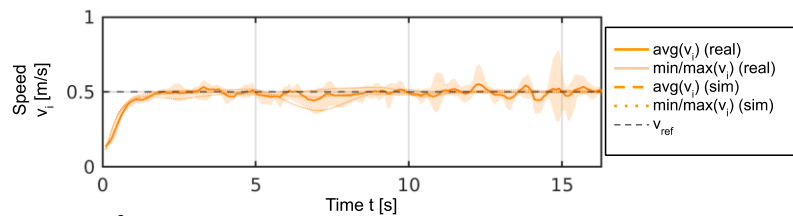
b



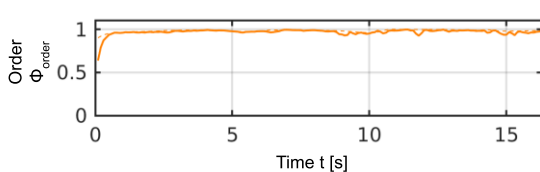
c



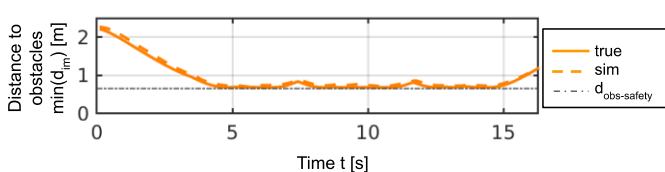
d



e



f



313  
314

315 **Fig. 5: Real-world experiment of the NMPC swarm.** (a) The swarm, composed of five  
316 commercial palm-sized quadrotors, flies through cylindrical obstacles in a motion capture arena.  
317 The swarm crosses the region from the foreground ( $t = 0$  s) to the background ( $t = T$ ), while  
318 maintaining cohesion and avoiding the obstacles (see Supplementary Video 2). (b) Top view of  
319 the trajectories of the drones. For the real-world deployment, we selected obstacles with a  
320 smaller radius ( $r_{\text{obs}} = 0.30$  m) than in simulation ( $r_{\text{obs}} = 0.55$  m), but we used the same safety  
321 distance for collision avoidance as in simulation ( $d_{\text{obs-safety}} = 0.65$  m), which introduces a

322 safety margin of  $0.25\text{ m}$  from the physical obstacles (see Supplementary Table 4). **(c)** Average  
323 inter-agent distance and range with the real swarm (solid line and shaded region, respectively)  
324 and the simulated swarm (dashed and dotted lines, respectively). **(d)** Average speed and range  
325 with the real swarm (solid line and shaded region, respectively) and the simulated swarm  
326 (dashed and dotted lines, respectively). **(e)** Swarm’s order: real (solid line) and simulated  
327 (dashed line) swarm. **(f)** Swarm distance to obstacles. The offset in the real data (solid line) with  
328 respect to the simulated data (dashed line) is due to the safety margin.

329  
330 We validated the NMPC swarm on five commercial quadrotors in an indoor motion capture  
331 arena where we reconstructed the environment described in Sec. 2.1 (Fig. 5a). We measured  
332 the real flight performance, and we compared them with the simulation performance. The real  
333 drones achieve the preferred inter-agent distance  $d_{\text{ref}} = 0.8\text{ m}$  with an error ( $E_d = 0.12 \pm 0.02$ )  
334 comparable to the simulation error ( $E_d = 0.11 \pm 0.02$ ) (Fig. 5c). However, the speed error is  
335 slightly higher ( $E_v = 0.07 \pm 0.03$ ) than in simulation ( $E_v = 0.02 \pm 0.02$ ) (Fig. 5d). The higher  
336 speed error in the real swarm can be explained by small communication delays and air  
337 turbulence due to the proximity of the drones to each other and obstacles. The order of the real  
338 swarm ( $\Phi_{\text{order}} = 0.97 \pm 0.04$ ) is comparable to the simulated swarm ( $\Phi_{\text{order}} = 0.98 \pm 0.02$ )  
339 (Fig. 5e), and in both cases we did not observe collisions ( $\Phi_{\text{agent-safety}} = 1 \pm 0$ ,  $\Phi_{\text{obs-safety}} =$   
340  $1 \pm 0$ ) (Fig. 5f).

### 342 **3 Discussion**

343  
344 This article shows that a Nonlinear Model Predictive Control (NMPC) model achieves a faster  
345 and more synchronized flight in cluttered environments as compared to state-of-the-art models  
346 based on potential fields (PFs). NMPC swarms report no collisions in cluttered environments,  
347 they better attain and maintain target speeds, and they remain more ordered and cohesive. The  
348 benefits brought by predictive controllers to robotic aerial swarms confirm a parallel with  
349 biological systems, where individuals are thought to enhance their synchronization by future  
350 state projection [19].

351  
352 In robotics, the advantages of the NMPC method are promising for applications that require  
353 navigation in crowded scenarios, such as the exploration of urban environments, collapsed  
354 buildings, or forests [45], [46]. Also, vision-based swarms could benefit from all these features  
355 since the reliability of reciprocal visual detection of the drones strongly depends on their  
356 distance, and NMPC swarms showed that they can better maintain target inter-agent distances  
357 [22], [47]. Overall, predictive methods can improve the autonomy of swarm operations as well  
358 as the safety of the swarm and the environment, which are both essential elements to build  
359 public confidence in the use of swarms [48].

360  
361 For our experiments, we relied on a central computing node that generates the motion of the  
362 agents at run time according to local interactions only. This assumption simplifies the  
363 implementation since it requires only one computer, acting as a ground control station, instead  
364 of several onboard computers that the agents would carry. However, the NMPC model requires  
365 a higher amount of computational resources than the PF model and scales worse with the

366 swarm size. It will be interesting to develop a decentralized NMPC model where the  
367 computational costs are independent of the number of agents. Work in this direction will allow  
368 to scale our approach to swarms of larger size.

369  
370 Finally, our results motivate future works to address research questions in the design of robust  
371 swarm models in dynamic environments. Thanks to their recursive structure, MPC controllers  
372 offer a promising method to allow navigation in scenarios with moving obstacles. However, a  
373 generalization of the proposed model to dynamic environments would require theoretical and  
374 numerical investigation on the conditions for stability, as well as a reliable estimation of the  
375 obstacles' motion [49].

376

## 377 **4 Methods**

378

379 In this work, we consider a swarm of  $N$  agents labeled by  $i \in \{1, \dots, N\}$ . The position, velocity,  
380 and control input of the  $i$ -th agent are denoted by  $\mathbf{p}_i, \mathbf{v}_i, \mathbf{u}_i \in \mathbb{R}^3$ , respectively. Let  $d_{ij} = \|\mathbf{p}_j - \mathbf{p}_i\|$   
381 represent the distance between the center of two agents  $i$  and  $j$ , where  $\|\cdot\|$   
382 denotes the Euclidean norm. We model the swarm with a directed sensing graph  $\mathcal{G} = (\mathcal{V}, \mathcal{E})$ ,  
383 where the vertex set  $\mathcal{V} = \{1, \dots, N\}$  represents the agents, and the edge set  $\mathcal{E} \subseteq \mathcal{V} \times \mathcal{V}$   
384 contains the pairs of agents  $(i, j) \in \mathcal{E}$  for which agent  $i$  can sense agent  $j$ . We denote as  
385  $\mathcal{N}_i = \{j \in \mathcal{V} \mid (i, j) \in \mathcal{E}\} \subset \mathcal{V}$  the set of neighbors of an agent  $i$  in  $\mathcal{G}$ , and  $|\cdot|$  indicates the  
386 cardinality of a set. We define the neighbors set utilizing a topological range, i.e., the set  $\mathcal{N}_i$   
387 contains the  $|\mathcal{N}_i|$  nearest neighbors of agent  $i$ . This choice is convenient for keeping the  
388 cardinality of the neighbor set constant, and it has also been shown to hold true for biological  
389 swarms [7]. Other studies have investigated different neighborhood approaches based on the  
390 Voronoi partition or ad-hoc attraction topologies [50]-[51]. However, we discarded those  
391 methods because they would introduce discontinuities in the objective function of our  
392 predictive swarm model, or they would constrain the swarm to a fixed formation. To reproduce  
393 a forest-like environment, we introduce  $M$  cylindrical obstacles labeled by  $m \in \{1, \dots, M\}$ . We  
394 denote as  $d_{im}$  the distance between an agent  $i$  and the symmetry axis of cylinder  $m$ . In our  
395 simulations, the dynamics of the agents is reproduced in discrete time. We let  $\mathbf{p}_i(k), \mathbf{v}_i(k),$   
396  $\mathbf{u}_i(k) \in \mathbb{R}^3$  be the position, velocity, and control input of the  $i$ -th agent at the time  $t(k) =$   
397  $k dt$ , respectively. For brevity, in the following we will omit the time dependency when clear  
398 from the context.

399

### 400 **4.1 PF swarm model**

401

402 The PF model we present is inspired by a state-of-the-art model that allows drone swarm  
403 navigation in confined environments [24]. From the original model, we include the rule of  
404 *repulsion* to prevent inter-drone collisions, *friction* to reduce velocity oscillations, and *obstacle*  
405 *avoidance* to avoid collisions with obstacles. For the mathematical definition of these rules, we  
406 refer the reader to [24]. To ensure goal-directed flight in open environments, we added two  
407 rules: *migration* to provide a preferred velocity vector, and *cohesion* to keep agents together.  
408 We denote the migration velocity with  $\mathbf{v}_{\text{ref}} = v_{\text{ref}} \mathbf{u}_{\text{ref}}$ , where  $v_{\text{ref}}$  is the preferred speed and

409  $\mathbf{u}_{\text{ref}}$  is the preferred direction. Then, the migration term, equal for every agent, corresponds to:

$$410 \quad \mathbf{v}_{\text{mig}} = v_{\text{ref}} \mathbf{u}_{\text{ref}} \quad (1)$$

411 If the repulsion is active when neighboring agents are closer than the preferred distance  $d_{\text{ref}}$   
 412 and push them further apart, the cohesion is active when they are farther than  $d_{\text{ref}}$  to bring  
 413 them closer. Repulsion and cohesion are inactive when two agents are precisely at the distance  
 414  $d_{\text{ref}}$ . The cohesion exerted on an agent  $i$  from a neighbor  $j$  is:

$$415 \quad \mathbf{v}_{\text{coh},ij} = \begin{cases} c_{\text{coh}}(d_{ij} - d_{\text{ref}}) \frac{\mathbf{p}_j - \mathbf{p}_i}{d_{ij}} & \text{if } d_{ij} < d_{\text{ref}} \\ 0 & \text{otherwise} \end{cases} \quad (2)$$

416 where we choose the pairwise gain of cohesion equal to the repulsion gain  $c_{\text{coh}} = c_{\text{rep}}$  and the  
 417 cutoff for the minimum cohesion range equal to the repulsion range  $d_{\text{ref}}$ . The total cohesion  
 418 effect calculated for agent  $i$  with respect to its neighbors is:

$$419 \quad \mathbf{v}_{\text{coh},i} = \sum_{j \in \mathcal{N}_i} \mathbf{v}_{\text{coh},ij} \quad (3)$$

420 At any instant, the velocity for agent  $i$  resulting from the contributions above is:

$$421 \quad \tilde{\mathbf{v}}_i = \mathbf{v}_{\text{mig}} + \mathbf{v}_{\text{coh},i} + \mathbf{v}_{\text{rep},i} + \mathbf{v}_{\text{fric},i} + \sum_{s \in M_i} \mathbf{v}_{\text{obstacle},is} \quad (4)$$

422  
 423 After summing the contributions, we apply a cutoff on the acceleration at  $a_{\text{max}}$  according to:

$$424 \quad \mathbf{a}_i = \frac{\tilde{\mathbf{a}}_i}{\|\tilde{\mathbf{a}}_i\|} \min(\|\tilde{\mathbf{a}}_i\|, a_{\text{max}}) \quad (5)$$

425 where  $\tilde{\mathbf{a}}_i(k+1) = (\tilde{\mathbf{v}}_i(k+1) - \tilde{\mathbf{v}}_i(k))/dt$ . Then, we apply a cutoff on the speed at  $v_{\text{max}}$ ,  
 426 and get the velocity command  $\mathbf{v}_i$  of the  $i$ -th agent:

$$427 \quad \mathbf{v}_i = \frac{\tilde{\mathbf{v}}_i}{\|\tilde{\mathbf{v}}_i\|} \min(\|\tilde{\mathbf{v}}_i\|, v_{\text{max}}) \quad (6)$$

428  
 429 To search the large parameter space of the PF swarm model, we used evolutionary optimization  
 430 for highest-order flight and lowest number of collisions. The evaluation of the swarm behavior is  
 431 based on a single fitness function that sums three independent values ( $\Phi_{\text{order}}$ ,  $\Phi_{\text{agent-safety}}$ ,  
 432 and  $\Phi_{\text{obs-safety}}$ ) smaller or equal to 1 (ideal case). The fitness is determined in simulations  
 433 where the swarm is initialized with random positions in an environment where obstacles are  
 434 randomly placed. The parameter values and their description are detailed in the Supplementary  
 435 Materials.

## 437 4.2 Agents' dynamics

438  
 439 The NMPC swarm model supposes the availability of the agents' dynamic model. We assume  
 440 that every drone of the swarm obeys a discrete linear system, given by:

$$441 \quad \mathbf{x}_i(k+1) = A_i \mathbf{x}_i(k) + B_i \mathbf{u}_i(k) \quad (7)$$

442 where  $A_i$  and  $B_i$  are constant matrices. In this article, we consider the system to represent a  
 443 quadrotor with an underlying acceleration controller. The input  $\mathbf{u}_i$  is an acceleration command  
 444 and the state  $\mathbf{x}_i = [\mathbf{p}_i, \mathbf{v}_i] \in \mathbb{R}^6$  is a vector containing the position and velocity.

445  
 446 We assume that the velocities and acceleration inputs of the agents are bounded by constant  
 447 vectors  $\mathbf{v}_{\text{min}}, \mathbf{v}_{\text{max}}$  and  $\mathbf{u}_{\text{min}}, \mathbf{u}_{\text{max}}$  respectively. This translates into the inequalities

$$448 \quad \mathbf{v}_{\text{min}} \leq \mathbf{v}_i(k) \leq \mathbf{v}_{\text{max}} \quad (8)$$

$$449 \quad \mathbf{u}_{\text{min}} \leq \mathbf{u}_i(k) \leq \mathbf{u}_{\text{max}} \quad (9)$$

450

451 Let  $\mathbf{x} = [\mathbf{x}_1, \mathbf{x}_2, \dots, \mathbf{x}_N] \in \mathbb{R}^{6N}$  the positions and velocities of the agents of the swarm, and  
 452  $\mathbf{u} = [\mathbf{u}_1, \mathbf{u}_2, \dots, \mathbf{u}_N] \in \mathbb{R}^{3N}$ . The system defining the motion of the swarm can be written as:

$$453 \quad \mathbf{x}(k+1) = A\mathbf{x}(k) + B\mathbf{u}(k) \quad (10)$$

454 where  $A$  and  $B$  are block diagonal matrices with blocks  $A_1, \dots, A_N$  and  $B_1, \dots, B_N$ ,  
 455 respectively. Parameter values of the agents' dynamics are detailed in the Supplementary  
 456 Materials.

457

### 458 4.3 NMPC swarm model

459

460 For our NMPC swarm model, we defined behavioral rules similar to those of the PF model.  
 461 These rules are encoded as four terms of a cost function, including *separation*, *propulsion*,  
 462 *direction*, and *control effort*. At each time step, each agent updates its neighbor set and  
 463 computes the cost associated with the four swarm rules only considering neighboring agents. All  
 464 agents' contributions are then summed in a global cost function that defines our centralized  
 465 model. The dynamic model of the agents introduced in Sec. 4.2. determines the evolution of the  
 466 agents' state over a constant time window, called the *prediction horizon*. These predictions are  
 467 optimized by the global cost function, whose solution gives the control inputs for the swarm  
 468 over the so-called *control horizon* (see Supplementary Fig. 3). The prediction and control  
 469 horizons are finite and shift forward at every time step. In the following, they will be denoted as  
 470  $T_p = P \, dt$  and  $T_c = C \, dt$  respectively, with  $P \geq C$  and  $P, C \in \mathbb{N}^+$ .

471

472 We let  $(\cdot)(k+l|k)$  represent the predicted value of  $(\cdot)(k+l)$  with the information  
 473 available at time  $t(k)$  and  $l \in \{0, \dots, P\}$ . Then, the continuity condition on the swarm state is  
 474 written as:

$$475 \quad \mathbf{x}(k|k) = \mathbf{x}(k) \quad (11)$$

476 The *separation* term for agent  $i$  and time  $t(k)$  is:

$$477 \quad J_{\text{sep},i}(k) = \sum_{j \in \mathcal{N}_i} \sum_{l=1}^P \frac{w_{\text{sep}}}{|\mathcal{N}_i|} \left( \|\mathbf{p}_j(k+l|k) - \mathbf{p}_i(k+l|k)\|^2 - d_{\text{ref}}^2 \right)^2 \quad (12)$$

478 The separation component incorporates the effects of cohesion and repulsion, and drives the  
 479 inter-agent distances to the preferred value  $d_{\text{ref}}$ . It is important to notice that commanding  
 480 inter-agent distances instead of relative positions, as done in problems of formation keeping  
 481 [33]-[34], [36]-[37], introduces a non-convexity in the separation term.

482 The *propulsion* term is:

$$483 \quad J_{\text{prop},i}(k) = \sum_{l=1}^P w_{\text{prop}} \left( \|\mathbf{v}_i(k+l|k)\|^2 - v_{\text{ref}}^2 \right)^2 \quad (13)$$

484 The *direction* term:

$$485 \quad J_{\text{dir},i}(k) = \sum_{l=1}^P w_{\text{dir}} \left( 1 - \frac{(\mathbf{v}_i(k+l|k) \cdot \mathbf{u}_{\text{ref}})^2}{\|\mathbf{v}_i(k+l|k)\|^2} \right)^2 \quad (14)$$

486 The combined action of the propulsion (12) and direction (13) terms contribute to the so-called  
 487 migration behavior of the swarm that regulate the two components of the swarm's velocity, i.e.,  
 488 magnitude and direction, respectively. The choice of two separate terms that independently act  
 489 on the swarm's velocity components is necessary to maintain constant flight speed during  
 490 obstacle avoidance maneuvers. The *control effort* is:

$$491 \quad J_{u,i}(k) = \sum_{l=0}^{P-1} w_u \|\mathbf{u}_i(k+l|k)\|^2 \quad (15)$$

492 where  $w_{\text{sep}}$ ,  $w_{\text{prop}}$ ,  $w_{\text{dir}}$ , and  $w_u$  represent the constant weights associated with the cost  
 493 function terms.

494  
 495 To prevent the agents from colliding with their neighbors or the obstacles, we associated with  
 496 the cost function two sets of collision avoidance constraints:

$$497 \quad d_{ij}(k+l|k)^2 \geq d_{\text{agent-safety}}^2 \quad i \in \{1, \dots, N\}, j \in \mathcal{N}_i \quad (16)$$

$$498 \quad d_{im}(k+l|k)^2 \geq d_{\text{obs-safety}}^2 \quad i \in \{1, \dots, N\}, m \in \{1, \dots, M\} \quad (17)$$

499 where  $d_{\text{agent-safety}}$  is the safety distance between two agents' positions and  $d_{\text{obs-safety}}$  is  
 500 the safety distance that an agent should keep from the obstacle's position. While in this study  
 501 we consider collision avoidance with all obstacles (see Eq. 17), the model does not necessarily  
 502 require it. Indeed, the obstacles that do not interfere with the agents' predicted trajectories are  
 503 discarded by the optimization process. A strategy for reducing the number of constraints in the  
 504 model consists of considering only the subset of obstacles that are on the collision course with  
 505 the agents. While this strategy would represent an approximation of more comprehensive  
 506 modeling of all obstacles, as presented here, the advantages of the model-based approach  
 507 described in this paper would still hold.

508  
 509 We let  $\mathbf{X}(k) \in \mathbb{R}^{6NP}$  the stacked sequence of the predicted states  $\mathbf{x}(k+l|k)$  over the  
 510 horizon  $l \in \{1, \dots, P\}$  and  $\mathbf{U}(k) \in \mathbb{R}^{3NP}$  the stacked sequence of the predicted control inputs  
 511  $\mathbf{u}(p|k)$  over the horizon  $l \in \{0, \dots, P-1\}$ . Then, the terms of the cost function (see Eq. 12-  
 512 15), and the constraints (see Eq. 8-11 and 16-17) define the following non-convex optimization  
 513 problem:

$$\begin{aligned} & \min_{\mathbf{X}(k), \mathbf{U}(k)} \quad \sum_{i=1}^N (J_{\text{sep},i}(k) + J_{\text{prop},i}(k) + J_{\text{dir},i}(k) + J_{u,i}(k)) \\ & \text{subject to} \\ & \quad \mathbf{x}(k+l+1|k) = A\mathbf{x}(k+l|k) + B\mathbf{u}(k+l|k) \\ & \quad \mathbf{x}(k|k) = \mathbf{x}(k) \\ & \quad \mathbf{v}_{\min} \leq \mathbf{v}_i(k+l|k) \leq \mathbf{v}_{\max} \\ & \quad \mathbf{u}_{\min} \leq \mathbf{u}_i(k+l|k) \leq \mathbf{u}_{\max} \\ & \quad d_{ij}(k+l|k)^2 \geq d_{\text{agent-safety}}^2 \\ & \quad d_{im}(k+l|k)^2 \geq d_{\text{obs-safety}}^2 \end{aligned} \quad (18)$$

514  
 515 with  $l \in \{1, \dots, P\}$ ,  $i \in \{1, \dots, N\}$ ,  $j \in \mathcal{N}_i$ , and  $m \in \{1, \dots, M\}$ .

#### 516 517 **4.4 Simulation setup**

518  
 519 We implemented our NMPC model in MATLAB with the help of acados [52], an open-source  
 520 library for fast nonlinear optimal control. This software relies on C code generation for speeding  
 521 up the computation in real-time applications. The system dynamics and the constraints of the  
 522 problem are discretized by the library over the prediction horizon to obtain a structured  
 523 Nonlinear Program (NLP). Then, the NLP is approximated through Sequential Quadratic  
 524 Programming (SQP) that iteratively solves convex Quadratic Program (QP) sub-problems. After  
 525 applying a condensing step, a linear algebra solver, HPIPM, based on the Interior Point (IP)  
 526 method finds the solution of the sub-problems [53]. We run our simulations on a DELL Precision

527 Tower with a 3.6 GHz Intel Core i7-7700 processor and 16 GB 2400 MHz RAM, where we set the  
528 maximum number of SQP to 7 and the maximum number of QP iterations to 7.

529

## 530 **4.5 Drone experimental setup**

531

532 In our experiments, we used five Bitcraze Crazyflie 2.1 quadrotors (Fig. 1c). Each quadrotor is  
533 equipped with a 3-axis accelerometer, a 3-axis gyroscope, a pressure sensor, and a marker deck  
534 for hosting passive reflective markers. The microcontroller is a STM32F4 running at 168MHz, on  
535 which both state estimation and low-level control are running. An OptiTrack motion capture  
536 system was used to track the position of the robots. All the acceleration commands for the  
537 drones were computed on a single computer with our NMPC model, integrated into position  
538 and velocity commands, and broadcast to the swarm through a radio-link alongside the  
539 estimated position of each drone. The estimated positions were used by the drones to perform  
540 the lower-level control loops and track the commands sent. The positions and velocities used by  
541 the swarm model were predicted with the agents' dynamic model. To guarantee the  
542 transferability of the NMPC swarm model to hardware experiments, we decreased the number  
543 of maximum SQP to 4. This was sufficient to compute converging solutions of the NLP in less  
544 than 0.1 s.

545

## 546 **Data availability**

547

548 Complementary data for reproducing the experiments are available in the Supplementary  
549 Materials. Simulation and hardware experimental data that supports the findings of this study  
550 can be downloaded from [54].

551

## 552 **Code availability**

553

554 The code that supports the findings of this study can be downloaded from [55].

555

## 556 **References**

557

- 558 [1] I. D. Couzin, J. Krause, N. R. Franks, and S. A. Levin, "Effective leadership and decision-  
559 making in animal groups on the move", *Nature*, vol. 433, pp. 513-516, 2005
- 560 [2] H. Hildenbrandt, C. Carere, and C. K. Hemelrijk, "Self-organized aerial displays of  
561 thousands of starlings: a model", *Behav. Ecol.*, vol. 21, no. 6, pp. 1349–1359, 2010
- 562 [3] G. F. Young, L. Scardovi, A. Cavagna, I. Giardina, and N. E. Leonard, "Starling Flock  
563 Networks Manage Uncertainty in Consensus at Low Cost", *PLOS Comput. Biol.*, vol. 9, no. 1, p.  
564 e1002894, 2013
- 565 [4] G. Dell'Araccia, G. Dell'Omo, D. P. Wolfer, and H.-P. Lipp, "Flock flying improves pigeons'  
566 homing: GPS track analysis of individual flyers versus small groups", *Anim. Behav.*, vol. 76, no. 4,  
567 pp. 1165–1172, 2008
- 568 [5] M. Nagy, Z. Ákos, D. Biro, and T. Vicsek, "Hierarchical group dynamics in pigeon flocks,"  
569 *Nature*, vol. 464, no. 7290, pp. 890–893, 2010

- 570 [6] M. Yomosa, T. Mizuguchi, G. Vásárhelyi, and M. Nagy, “Coordinated Behaviour in Pigeon  
571 Flocks”, *PLOS ONE*, vol. 10, no. 10, p. e0140558, 2015
- 572 [7] M. Ballerini *et al.*, “Interaction ruling animal collective behavior depends on topological  
573 rather than metric distance: Evidence from a field study,” *Proc. Natl. Acad. Sci.*, vol. 105, no. 4,  
574 pp. 1232–1237, 2008
- 575 [8] D. Floreano and R. J. Wood, “Science, technology and the future of small autonomous  
576 drones”, *Nature*, vol. 521, no. 7553, pp. 460–466, 2015
- 577 [9] T. Stirling, J. Roberts, J.-C. Zufferey, and D. Floreano, “Indoor navigation with a swarm of  
578 flying robots”, *IEEE Int. Conf. Rob. Autom. (ICRA)*, pp. 4641–4647, 2012
- 579 [10] K. N. McGuire, C. D. Wagter, K. Tuyls, H. J. Kappen, and G. C. H. E. de Croon, “Minimal  
580 navigation solution for a swarm of tiny flying robots to explore an unknown environment,” *Sci.*  
581 *Robot.*, vol. 4, no. 35, p. eaaw9710, 2019
- 582 [11] A. T. Erman, L. van Hoesel, P. Havinga, and J. Wu, “Enabling mobility in heterogeneous  
583 wireless sensor networks cooperating with UAVs for mission-critical management”, *IEEE Wirel.*  
584 *Commun.*, vol. 15, no. 6, pp. 38–46, 2008
- 585 [12] A. Tagliabue, M. Kamel, R. Siegwart, and J. Nieto, “Robust collaborative object  
586 transportation using multiple MAVs,” *Int. J. Robot. Res.*, vol. 38, no. 9, pp. 1020–1044, 2019
- 587 [13] F. Augugliaro *et al.*, “The Flight Assembled Architecture installation: Cooperative  
588 construction with flying machines”, *IEEE Control Syst. Mag.*, vol. 34, no. 4, pp. 46–64, 2014
- 589 [14] “Intel Drone Light Show: Intel’s 50th Anniversary”,  
590 [https://www.intel.com/content/www/us/en/technology-innovation/videos/drone-light-show-](https://www.intel.com/content/www/us/en/technology-innovation/videos/drone-light-show-50th-anniversary-video.html)  
591 [50th-anniversary-video.html](https://www.intel.com/content/www/us/en/technology-innovation/videos/drone-light-show-50th-anniversary-video.html), 21 Nov. 2019
- 592 [15] “EHang Egret’s 1374 drones dancing over the City Wall of Xian, achieving a Guinness  
593 World Records title”, <https://www.ehang.com/news/365.html>, 02 May 2018
- 594 [16] “The Globe and Mail: Mini-drone use on the rise to light up big concerts like Celine Dion  
595 and Drake”, <https://veritystudios.com/news/globe-and-mail-celine>, 06 Dec. 2019
- 596 [17] D. Chen, X. Liu, B. Xu, and H.-T. Zhang, “Intermittence and connectivity of interactions in  
597 pigeon flock flights”, *Sci. Rep.*, vol. 7, no. 1, 2017
- 598 [18] A. Berdahl, C. J. Torney, C. C. Ioannou, J. J. Faria, and I. D. Couzin, “Emergent sensing of  
599 complex environments by mobile animal groups”, *Science*, vol. 339, no. 6119, pp. 574–576, 2013
- 600 [19] I. D. Couzin, “Synchronization: The Key to Effective Communication in Animal  
601 Collectives”, *Trends Cogn. Sci.*, vol. 22, no. 10, pp. 844–846, 2018
- 602 [20] C. W. Reynolds, “Flocks, Herds, and Schools: A Distributed Behavioral Model”, *Comput.*  
603 *Graph.*, vol. 21, pp. 25–43, 1987.
- 604 [21] S. Hauert *et al.*, “Reynolds Flocking in Reality with Fixed-Wing Robots: Communication  
605 Range vs. Maximum Turning Rate”, *IEEE/RSJ Int. Conf. Intell. Robots Syst. (IROS)*, pp. 5015-5020,  
606 2011
- 607 [22] F. Schilling, J. Lecoeur, F. Schiano, and D. Floreano, “Learning Vision-based Flight in  
608 Drone Swarms by Imitation”, *IEEE Robot. Autom. Lett.*, vol. 4, pp. 4523–4530, 2019
- 609 [23] R. Olfati-Saber, “Flocking for Multi-Agent Dynamic Systems: Algorithms and Theory,”  
610 *IEEE Trans. Autom. Control*, vol. 51, no. 3, pp. 401–420, 2006
- 611 [24] G. Vásárhelyi, C. Virágh, G. Somorjai, T. Nepusz, A. E. Eiben, and T. Vicsek, “Optimized  
612 flocking of autonomous drones in confined environments”, *Sci. Rob.*, vol. 3, no. 20, p. eaat3536  
613 2018

- 614 [25] G. Vasarhelyi *et al.*, “Outdoor flocking and formation flight with autonomous aerial  
615 robots”, *IEEE/RSJ Int. Conf. Intell. Robots Syst. (IROS)*, pp. 3866–3873, 2014
- 616 [26] Y. Koren and J. Borenstein, “Potential field methods and their inherent limitations for  
617 mobile robot navigation”, *IEEE Int. Conf. Rob. Autom. (ICRA)*, pp. 1398–1404, 1991
- 618 [27] E. Soria, D. Floreano, and F. Schiano, “The influence of limited visual sensing on the  
619 Reynolds flocking algorithm”, *Int. Conf. Rob. Comp. (IRC)*, pp. 138–145, 2019
- 620 [28] F. Borrelli, A. Bemporad, and M. Morari, “Predictive Control for Linear and Hybrid  
621 Systems”, 1st ed. Cambridge University Press, 2017
- 622 [29] L. Grune and J. Pannek, “Nonlinear Model Predictive Control. Theory and Algorithms”,  
623 Springer London, 2011
- 624 [30] T. Baca, D. Hert, G. Loianno, M. Saska, and V. Kumar, “Model Predictive Trajectory  
625 Tracking and Collision Avoidance for Reliable Outdoor Deployment of Unmanned Aerial  
626 Vehicles”, *IEEE/RSJ Int. Conf. Intell. Robots Syst. (IROS)*, pp. 6753–6760, 2018
- 627 [31] D. Falanga, P. Foehn, P. Lu, and D. Scaramuzza, “PAMPC: Perception-Aware Model  
628 Predictive Control for Quadrotors”, *IEEE/RSJ Int. Conf. Intell. Robots Syst. (IROS)*, pp. 1-8, 2018
- 629 [32] C. E. Luis, M. Vukosavljev, and A. P. Schoellig, “Online Trajectory Generation With  
630 Distributed Model Predictive Control for Multi-Robot Motion Planning”, *IEEE Robot. Autom.  
631 Lett.*, vol. 5, no. 2, pp. 604–611, 2020
- 632 [33] T. Keviczky, F. Borrelli, K. Fregene, D. Godbole, and G. J. Balas, “Decentralized Receding  
633 Horizon Control and Coordination of Autonomous Vehicle Formations”, *IEEE Trans. Control Syst.  
634 Technol.*, vol. 16, no. 1, pp. 19–33, 2008
- 635 [34] Ruben Van Parys, “Distributed MPC for multi-vehicle systems moving in formation”,  
636 *Robot. Autom. Syst.*, 2017
- 637 [35] U. Eren, A. Prach, B. B. Koçer, S. V. Raković, E. Kayacan, and B. Açıkmeşe, “Model  
638 Predictive Control in Aerospace Systems: Current State and Opportunities”, *J. Guid. Control  
639 Dyn.*, vol. 40, no. 7, pp. 1541–1566, 2017
- 640 [36] W. B. Dunbar and R. M. Murray, “Distributed receding horizon control for multi-vehicle  
641 formation stabilization”, *Automatica*, vol. 42, no. 4, pp. 549–558, 2006
- 642 [37] R. L. Raffard, C. J. Tomlin, and S. P. Boyd, “Distributed optimization for cooperative  
643 agents: application to formation flight”, *IEEE Conf. Decision Control (CDC)*, vol. 3, pp. 2453-2459 ,  
644 2004
- 645 [38] T. Schouwenaars, J. How, and E. Feron, “Decentralized Cooperative Trajectory Planning  
646 of Multiple Aircraft with Hard Safety Guarantees”, *AIAA Guid. Nav. and Cont. Conf.*, 2004
- 647 [39] A. Richards and J. How, “Implementation of Robust Decentralized Model Predictive  
648 Control”, *AIAA Guid. Nav. and Cont. Conf.*, 2005
- 649 [40] Y. Kuwata and J. P. How, “Robust Cooperative Decentralized Trajectory Optimization  
650 using Receding Horizon MILP,” in *American Cont. Conf.*, pp. 522–527, 2007
- 651 [41] I. Kagan Erunsal, A. Martinoli, and R. Ventura, “Decentralized Nonlinear Model Predictive  
652 Control for 3D Formation of Multirotor Micro Aerial Vehicles with Relative Sensing and  
653 Estimation”, *Int. Symp. on Multi-Robot and Multi-Agent Syst. (MRS)*, pp. 176–178, 2019
- 654 [42] W. Zhao and T. H. Go, “Quadcopter formation flight control combining MPC and robust  
655 feedback linearization”, *J. Frankl. Inst.*, vol. 351, no. 3, pp. 1335–1355, 2014
- 656 [43] W. Ren and N. Sorensen, “Distributed coordination architecture for multi-robot  
657 formation control”, *Robot. Autom. Syst.*, vol. 56, no. 4, pp. 324–333, 2008

- 658 [44] M. Kamel, J. Alonso-Mora, R. Siegwart, and J. Nieto, "Robust collision avoidance for  
659 multiple micro aerial vehicles using nonlinear model predictive control", *IEEE/RSJ Int. Conf.*  
660 *Intell. Robots Syst. (IROS)*, pp. 236–243, 2017
- 661 [45] V. Kumar and N. Michael, "Opportunities and challenges with autonomous micro aerial  
662 vehicles," *Int. J. Robot. Res.*, vol. 31, no. 11, pp. 1279–1291, 2012
- 663 [46] M. Petrlík, T. Báča, D. Heřt, M. Vrba, T. Krajník, and M. Saska, "A Robust UAV System for  
664 Operations in a Constrained Environment", *IEEE Robot. Autom. Lett.*, vol. 5, no. 2, pp. 2169–  
665 2176, 2020
- 666 [47] K. R. Sapkota *et al.*, "Vision-based Unmanned Aerial Vehicle detection and tracking for  
667 sense and avoid systems," *IEEE/RSJ Int. Conf. Intell. Robots Syst. (IROS)*, pp. 1556–1561, 2016
- 668 [48] E. R. Hunt and S. Hauert, "A checklist for safe robot swarms", *Nat. Mach. Intell.*, vol. 2,  
669 no. 8, pp. 420–422, 2020
- 670 [49] B. Lindqvist, S. S. Mansouri, A. Agha-mohammadi, and G. Nikolakopoulos, "Nonlinear  
671 MPC for Collision Avoidance and Control of UAVs With Dynamic Obstacles," *IEEE Robot. Autom.*  
672 *Lett.*, vol. 5, no. 4, pp. 6001–6008, 2020
- 673 [50] A. Strandburg-Peshkin *et al.*, "Visual sensory networks and effective information transfer  
674 in animal groups", *Curr. Biol.*, vol. 23, no. 17, pp. 709-711, 2013
- 675 [51] Z. Chen, T. Chu, "Multi-agent system model with mixed coupling topologies for pattern  
676 formation and formation splitting", *Math. Comput. Model. Dyn. Syst.*, vol. 19, pp. 388-400, 2013
- 677 [52] R. Verschueren *et al.*, "Towards a modular software package for embedded  
678 optimization", *IFAC-Pap.*, vol. 51, no. 20, pp. 374–380, 2018
- 679 [53] G. Frison, D. K. M. Kufoalor, L. Imsland, and J. B. Jørgensen, "Efficient implementation of  
680 solvers for linear model predictive control on embedded devices", *IEEE Conf. Control Applic.*  
681 *(CCA)*, pp. 1954-1959, 2014
- 682 [54] E. Soria, F. Schiano, and D. Floreano, "Predictive control of aerial swarms in cluttered  
683 environments", *Zenodo*, 2020, <https://doi.org/10.5281/zenodo.4379168>
- 684 [55] E. Soria, F. Schiano, and D. Floreano, "Predictive control of aerial swarms in cluttered  
685 environments", *Zenodo*, 2020, <https://doi.org/10.5281/zenodo.4379503>
- 686

## 687 Correspondence

688  
689 Correspondence and requests for materials should be addressed to E. S.  
690

## 691 Acknowledgments

692  
693 We thank A. De Bortoli, M. Pfister, and F. Schilling for the helpful discussions. This work was  
694 supported by the Swiss National Science Foundation with grant number 200020\_188457. This  
695 work was also partially funded by the European Union's Horizon 2020 research and innovation  
696 programme under grant agreement ID: 871479 AERIAL-CORE.  
697

## 698 Author contributions

699  
700 All authors contributed to the conception of the project and were involved in the analysis of the

701 results. E.S. has designed, implemented, and performed software and hardware experiments of  
702 the NMPC algorithm for the navigation of drone swarms in cluttered environments. All authors  
703 contributed to the writing of the manuscript.

704

### 705 **Competing interests**

706

707 The authors declare that they have no competing interests.

708